Clusters and Lattices of Particles Stabilized by Dipolar Coupling

Artem Baskin,[†] Wai-Yip Lo,[†] and Petr Král[†,‡,*]

[†]Department of Chemistry and [‡]Department of Physics, University of Illinois at Chicago, Illinois 60607, United States

ABSTRACT

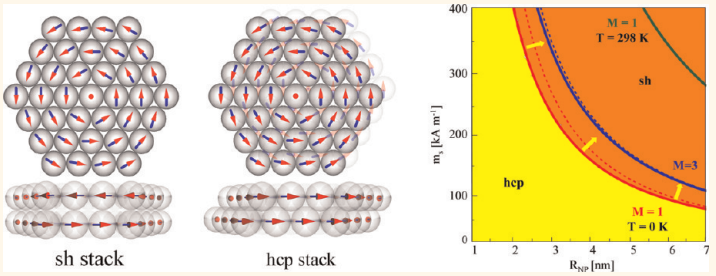

We model stabilization of clusters and lattices of spherical particles with dominant electric and magnetic dipolar coupling, and weak van der Waals coupling. Our analytical results demonstrate that dipolar coupling can stabilize nanoparticle clusters with planar, tubular, Möbius, and other arrangements. We also explain for which parameters the nanoparticles can form lattices with fcc, hcp, sh, sc, and other types of packing. Although these results are valid at different scales, we illustrate that realistic magnetic and semiconducting nanoparticles need to have certain minimum sizes to stabilize at room temperature into nanostructures controlled by dipolar coupling.

KEYWORDS: clusters · dipolar coupling · stabilization · nanostructures

In recent years, colloidal nanoparticles (NP) of different materials,[1,2] shapes,[3−6] and ligations[7−10] have been self-assembled into superlattices with many types of packing.[11−23] It is crucial to understand the principles underlying their self-assembly[24] to predict and control the structures formed.[25] The interparticle forces that lead to these structures originate in the bulk and surface characteristics of the colloidal NPs.[8,26−29] When the bulk forces dominate in the NP self-assembly, we might described them by averaged force-fields acting between the NPs.[22,30−35] Otherwise, we need to model the NPs atomistically and pay attention to their ligands.[36]

Among the many prepared systems, clusters and lattices of NPs stabilized by coupled electric[31,35,37] and magnetic[38−41] dipoles have been observed. It turns out that the type of structures formed depends on the number of particles and the relative strength of the anisotropic dipole−dipole coupling and the isotropic van der Waals (vdW) coupling. If the relative strength of coupling is fixed and the number of particles is increased, the Stockmayer model predicts the formation of perfect icosahedra, entangled knots, linear chains, and planar rings.[42] On substrates, colloidal magnetic NPs (MNPs) at low densities were seen to form lines and rings, while at high densities, they form chains and bandlike aggregates.[43−46]

The types of lattices stabilized should depend on the strength of dipolar coupling. At weak dipolar coupling, the vdW coupling dominates and leads to closed-packed fcc and hcp lattices.[23,35,47−49] As the strength of dipolar coupling increases, the dipoles can form ordered structures at room temperatures.[14,50] At large (dominant) dipolar coupling, the vdW coupling becomes irrelevant. Then, one should observe the formation of lattices with looser arrangement of NPs, such as simple hexagonal (sh) lattices of PbSe semiconducting NPs with electric dipoles[35] or nearly close-packed assemblies of Co nanocrystals and Rh_4H_2 atomic magnetic clusters.[14,51] The stabilization conditions of particle clusters might also depend on the substrate used for their deposition.[52] Various intricate spatial spin configurations were predicted to exist in ultrathin films, such as the presence of magnetic vortices.[53] The question is if such complex dipolar arrangements can also be prepared in NP systems.

In this work, we systematically investigate clusters and lattices stabilized by electric or magnetic dipolar coupling of their particle constituents. Despite the formal similarity of NPs with electric and magnetic coupling, the absence of magnetic charges make them rather different.[35,54] Typically, the self-assembly of colloidal NPs with electric dipoles can be largely influenced by screening in ionic solutions. On the other hand, magnetic dipolar interactions are relatively weak, but less

* Address correspondence to pkral@uic.edu.

Received for review March 15, 2012 and accepted June 8, 2012.

Published online June 08, 2012
10.1021/nn301155c

spatially limited, due to lack of magnetic screening. MNPs can also have more complex coupling, since they interact at different length scales by dipole−dipole, magnetic anisotropy, and exchange mechanisms[7,55−58] The atomic exchange interaction acts at the length scale of 10 nm,[43,59] which is about the size of MPs for which this coupling matters.[60] The magnetic anisotropy and the MNP-shape are also important factors guiding the self-assembly.[61] However, magnetic anisotropy is of less relevance for freely rotating MPs. Thus, dipolar coupling dominates in the formation of structures with 10−100 nm MPs,[62−67] with rich potential applications.[68]

METHODS

We will calculate the energies of assembled particles with dipolar coupling in different clusters and lattices. The dipole−dipole interaction energy between the i and j particles located at the $\vec{x}_i$ and $\vec{x}_j$ positions, and having the dipoles $\vec{\mu}_i$ and $\vec{\mu}_j$, respectively, is

$$W_{ij} = \frac{\vec{\mu}_i \cdot \vec{\mu}_j - 3(\vec{n}_{ij} \cdot \vec{\mu}_i)(\vec{n}_{ij} \cdot \vec{\mu}_j)}{|\vec{x}_i - \vec{x}_j|^3} = \Lambda_{m(e)} w_{ij} \quad (1)$$

where $\vec{n}_{ij}$ is a unit vector in the $\vec{x}_i - \vec{x}_j$ direction. We can rewrite W_{ij} as a product of the unitless geometric factor, w_{ij}, and the effective magnetic and electric dipole−dipole interaction strengths, $\Lambda_m = \mu_0 \mu_m^2/(4\pi d^3)$ and $\Lambda_e = \mu_e^2/(4\pi\varepsilon_0 d^3)$, respectively. Here, $\mu_{m(e)}$ is the magnitude of the magnetic (electric) dipole moment, μ_0 is the magnetic permeability of vacuum, ε_0 is dielectric constant for vacuum, and d is the particle diameter.

The dipole moment of a spherical particle with homogeneous magnetization m_s per unit volume or ρ_s electric dipolar density are given by

$$\mu_m = \frac{\pi}{6} d^3 m_s, \quad \mu_e = \frac{\pi}{6} d^3 \rho_s \quad (2)$$

In our energy calculations, we will use the local dipole approximation, where we replace the material by point dipoles of the size, $\mu_{m(e)}$, located in the particle center. If its size scales as $d \rightarrow \alpha d$, the binding energy scales as $W \rightarrow \alpha^3 W$. This allows us to estimate the minimal size of the particles that form systems stable at room temperatures.

In the following, we consider different dipolar and lattice arrangements with N particles and calculate their total binding energies

$$E_{tot} = \sum_i \sum_{j>i} W_{ij} = \Lambda_{m(e)} \varepsilon$$
$$\varepsilon = \sum_i \sum_{j>i} w_{ij} = \sum_i \varepsilon_i = \bar{\varepsilon} N \quad (3)$$

We find the relative stability of different particle assemblies by evaluating the average energy factor per particle, $\bar{\varepsilon}$.

The model in eq 3 describes anisotropic dipole−dipole coupling between spherical particles. When the dipolar coupling is strong, such as in Co nanocrystals[14] and ionic colloidal microparticles,[69] this coupling alone can determine the lattice structure. If other interparticle coupling mechanisms are relevant they can be added in the model as well.[36] Here, we estimate the effect of isotropic vdW interactions between the spherical particles using the formula[32,70]

$$W_{ij}^{vdW} = -\left(\frac{A}{12 d_{ij}(1 + d_{ij}/4R)} + \frac{1}{1 + d_{ij}/R + d_{ij}^2/4R^2} + 2 \ln\left(\frac{d_{ij}(1 + d_{ij}/4R)}{R(1 + d_{ij}/R + d_{ij}^2/4R^2)} \right) \right) \quad (4)$$

Here, R is the particle radius, d_{ij} is the distance between the ith and jth nanoparticles, and A is the Hamaker constant.

At finite temperatures, the stability of different particle arrangements (phases) is determined by their free energies. To find out which of the (two) possible phases is more stable at a given temperature T and pressure P, we can evaluate the change of the Gibbs free energy associated with the transition between the arrangements, $\Delta G = \Delta U + P\Delta V - T\Delta S$, where U is the potential energy (E in eq 3), V is the volume, and S is the entropy of each arrangement.

RESULTS AND DISCUSSION

Planar Arrangements of Dipolar Particles. Recently, superlattices of spherical colloidal PbSe NPs were observed to form loose sh packing on conductive substrates, and explained by vertical antiferroelectric dipolar ordering.[35] However, the proposed dipolar organizations may not be the most stable. Moreover, other dipolar planar structures might allow stabilization of NPs with different lattice arrangements. We study planar systems with different dipolar and lattice structures, compare their energies using eq 3, and check their stabilization with large magnetic particles (see Figure 7).

Magnetic structures with closed fluxes, such as rings and other more complex arrangements, tend to be highly stable.[50,54,59,71,72] Therefore, we will investigate first planar clusters and lattices with closed fluxes. In Figure 1 (top), we show closed-flux clusters which contain M circumcircles of dipoles oriented along a tangent to the circumcircle. The central dipole points up or down. Even though, we do not optimize the dipole orientations, the closed flux guarantees that their orientations are almost correct (for plaques of 2 and higher circumcircles the dipoles should not be exactly tangential). The clusters have a nonzero quadrupole moment and belong to the 6/*mmm* magnetic group symmetry.

Upon evaluation of the energy factor $\bar{\varepsilon}$ for the clusters in Figure 1 (top), we found that it is almost independent of M and approaches $\bar{\varepsilon} \rightarrow -2.7$. In an infinite chain of NPs with a head-to-tail orientation of

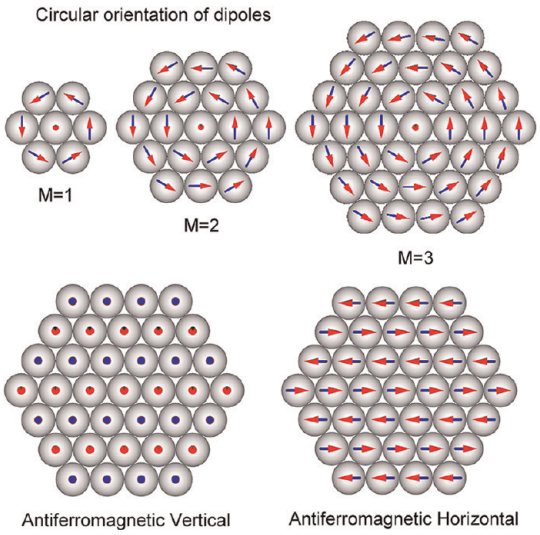

Figure 1. Honeycomb plaques of different sizes and orientation of dipoles, where *M* is the number of circumcircles.

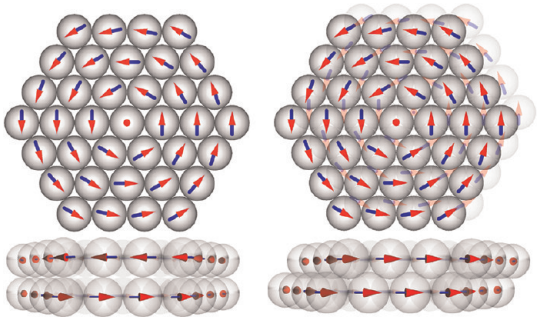

Figure 2. Stable configurations of particles and dipoles in two paralel plaques. (left) The simple hexagonal lattice with dipoles circulating in opposite directions in adjacent layers. (right) The hexagonal close-packed lattice with dipoles circulating in the same directions in the layers. Top views and side views are given.

dipoles, we obtain the asymptotic dependence of $\bar{\varepsilon}(N) = -2(\zeta(3) - (\pi^2/(6N))) \rightarrow -2.404$, where $\zeta(x)$ is the zeta function. It is useful to estimate at which sizes of NP the clusters in Figure 1 (top) are stable at room temperature, *i.e.*, $\Lambda\,\bar{\varepsilon} \approx 10$ kT. For the saturation magnetization of m_s = 425 kA m^{-1} in cobalt ferrite MNPs,[44,73,74] we obtain d_{crit} = 13.31, 11.97, 11.55 nm, while for CdSe NPs with the uniform dipolar density $\rho_s = 3.265 \times 10^{-3}$ C m^{-2}, we get d_{crit} = 9.61, 8.62, 8.34 nm (M = 1, 3, ∞).

Multilayers of Honeycomb Plaques. Next, we study multilayers of coupled honeycomb plaques. In Figure 2, we show two stable arrangements of honeycomb plaques placed on the top of each other. The total dipole−dipole interaction energies per particle of these clusters are summarized in Table 1. It is very interesting that when the dipoles are oriented in the same way within the layers, they tend to get closer and form the *hcp* (*fcc*) lattice, while if they are oriented in the opposite way, they tend to be further away and form the *sh* lattice. Moreover, the stability of these clusters depends on the size of the plaques. When the number of circumcircles exceeds 4, the hcp lattice becomes more stable than the sh lattice. This dipole organization might explain the experimentally observed lattices.[35]

TABLE 1. The Energy Factor Per Particle, $\bar{\varepsilon}$, in Multiple Layers of Identical Honeycomb Plaques with Different Orientations of Dipoles[a]

		circ: 1 (7)		circ: 2(19)		circ: 3(37)		circ: 4(61)	
layers	orientation	sh	hep	sh	hep	sh	hep	sh	hep
1		−1.76		−2.28		−2.45		−2.53	
2	same	−1.81	**−1.91**	−2.26	**−2.39**	−2.40	**−2.55**	−2.47	**−2.63**
	oppos.	**−1.98**	−1.81	**−2.41**	−2.22	**−2.55**	−2.38	**−2.62**	−2.45
3	same	−1.85	**−1.98**	−2.25	**−2.44**	−2.39	**−2.58**	−2.45	**−2.66**
	alt.	**−2.08**	−1.77	**−2.46**	−2.21	**−2.59**	−2.35	**−2.65**	−2.43
4	same	−1.88	**−2.02**	−2.25	**−2.46**	−2.38	**−2.60**	−2.44	**−2.67**
	alt.	**−2.13**	−1.79	**−2.48**	−2.20	**−2.61**	−2.34	**−2.66**	−2.41

[a] The top row horizontally arranged numbers show the circumcircles (circ.) (particles) in these clusters. The first column numbers (1−4) give the number of layers and the mutual dipole orientation in the neighboring layers. The bold numbers show dipole orientations with minimal energies.

It is also of interest to find out when the looser sh structure, stabilized here by the anisotropic dipole−dipole coupling, becomes destabilized by the isotropic vdW coupling between the particles to the extent that the structure switches to the hcp lattice arrangement. We briefly study the transition between the hcp and sh configurations in the double layer of honeycomb plaques (M = 1, 3) with the opposite direction of dipoles in each layer. We combine eqs 3−4 to evaluate the total energy of the two arrangements as a function of the particle radius R and the saturation magnetization m_s (strength of dipolar coupling). We use this energy (U) to evaluate the difference of the Gibbs free energy of the two phases, ΔG, where their entropy is approximated by the values obtained in bulk lattices (see below) and the pressure term $P\Delta V$ is neglected.

In Figure 3, we present the phase diagram of the two plaques calculated from ΔG, where the vdW coupling is characterized by the average Hamaker constant (metals) of A = 2.38 eV.[75] At zero temperature, the hcp configuration dominates (lower E) when the particle radius R or magnetization m_s are small, whereas the sh configuration prevails elsewhere. At larger plaques, the hcp arrangement becomes stable at larger R and m_s. To roughly simulate the presence of surfactants on the particles,[36] we also show by the dashed lines the results obtained for looser structures, where the distance between adjacent spherical particles is 1 nm. At higher temperatures, the larger entropy of the hcp configuration become significant, causing the phase transition to shift toward particles with larger R and m_s (larger coupling).

In our calculation of $\Delta G_{sh\rightarrow hcp}$, we have estimated the entropy for the sh and hcp arrangements using the known bulk values (per particle) in hard sphere

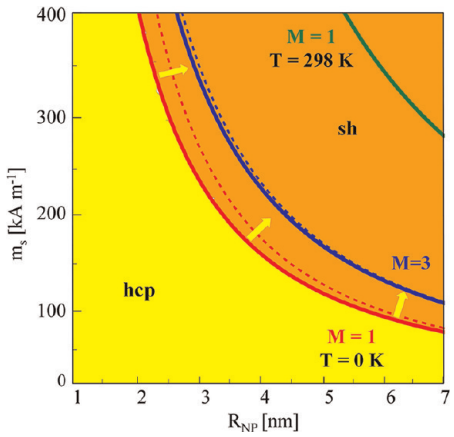

Figure 3. The phase diagram for magnetic NPs with a bulk vdW coupling plotted as a function of the NP-radius, R_{NP}, and the saturation magnetization, m_s. The NPs are arranged in two plaques with M = 1 and 3 circumferences and opposite orientations of dipole moments, which are positioned on the top of each other in the hcp and sh configurations. The solid lines represent the hcp/sh phase boundary of touching NPs, while the dashed lines give the phase boundary for NPs with the minimum separation of 1 nm (surfactants). When the temperature is raised to T = 298 K, the hcp/sh phase boundary shifts toward larger m_s and R_{NP} (stronger coupling), since the hcp configuration has a larger entropy.

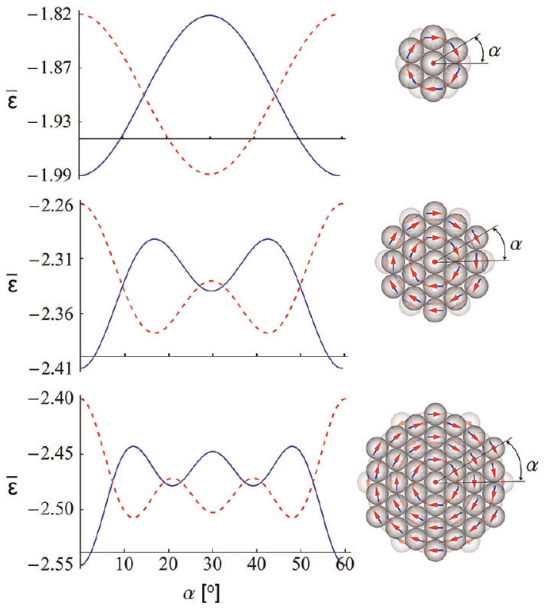

Figure 4. The potential energy per particle, $\bar{\varepsilon}$, in a double layer of honeycomb plaques of different sizes, rotated one with respect the other by the angle of α; M = 1 (up), M = 2 (middle), M = 3 (bottom). The α = 0 angle corresponds to the sh configuration. Solid and dashed curves correspond to the opposite and the same orientations of dipoles, respectively.

TABLE 2. The Energy Factors Per Particle, $\bar{\varepsilon}$, in Honeycomb Plaques with Different Orientation of Dipoles: Antiferromagnetic(Electric) Vertical (AV), Antiferromagnetic (Electric) Horizontal (AH) and Circular[a]

layers		circ. l(7)	2(19)	3(37)	4(61)
1	AV	−0.57	−0.69	−0.75	−0.79
	AH	**−1.26**	**−1.59**	**−1.72**	**−1.80**
2	AV,sh	−1.46	−1.54	−1.59	−1.62
	AV,hcp	−1.06	−1.15	−1.21	−1.23
	AH, sh	**−1.49**	**−1.75**	**−1.86**	**−1.93**
polarizable substrate	AV	−1.46	−1.54	−1.59	−1.62
	AH	−1.49	−1.75	−1.86	−1.93
	circular	**−1.99**	**−2.41**	**−2.55**	**−2.62**

[a] AV and AH double-layers with the sh and hcp lattices are considered. Bold numbers show the dipole orientations with a minimal energy.

crystals,[76−79] and replacing for simplicity $\Delta S_{sh\rightarrow hcp} \rightarrow -\Delta S_{fcc\rightarrow hcp} \approx 0.001\ k$ per particle. Using the enthalpy differences obtained in our systems, $\Delta H_{fcc\rightarrow hcp}$, and starting at T = 0 K in the sh phase in the phase diagram from Figure 3, we can find the critical NP size that would keep the system in this phase at a given temperature. At room temperature, the NPs with m_s = 425 kA m^{-1} must have the diameter $d > 5.2$, 5.8 nm for the plaques M = 1, 3, respectively, to prevent the transition to the more entropic hcp arrangement. For d = 10 nm, the enthalpy is already 10 times larger than the entropic term. If the vdW coupling is neglected, we can find that the critical size of NPs scales with temperature as $d_{min} \approx T^{1/3}$.

We can extend the stability analysis to systems with honeycomb plaques of antiferromagnetic (electric), vertical (AV), and horizontal (AH) orientation of dipoles, shown in Figure 1 (bottom).[35] Our results in Table 2 show that these dipolar open-flux arrangements are less stable than those discussed above; that is, the total energy per particle is $\bar{\varepsilon}_{circ} < \bar{\varepsilon}_{AH}\ \bar{\varepsilon}_{AV}$. Similar situation holds for a double layer. We tested both sh and hcp lattices and found that the AH sh configuration is the most stable, while the AH hcp configuration is not stable.

We also calculate the energies of these clusters on an ideally polarizable substrate. Although the circular orientation of dipoles provides the largest coupling energy per particle, the AV structures gives the strongest binding to the substrate, as found experimentally.[35] Even though the clusters with circular orientation of dipoles stabilized on the surface have the largest total binding energy per particle, we need to deposit them on the substrate already assembled, since individual NPs deposited on the surface prefer the vertical orientation. Therefore, controlling the kinetics of self-assembly is important for the design of materials with tailored properties. The kinetics depends on the substrate polarizability, the speed of solvent evaporation, the speed of particle aggregation, and other factors. Strong NP attraction to the substrate may prevent relaxation of the formed structures, resulting in malformed aggregates.[14,80]

It is of interest to investigate how the energies of the double-layer systems change when the layers are rotated and translated with respect to each other. We examine first two identical honeycomb plaques with the same or opposite dipole circulations in the sh configurations, and rotate them around the central particle. In Figure 4, we present the obtained potential

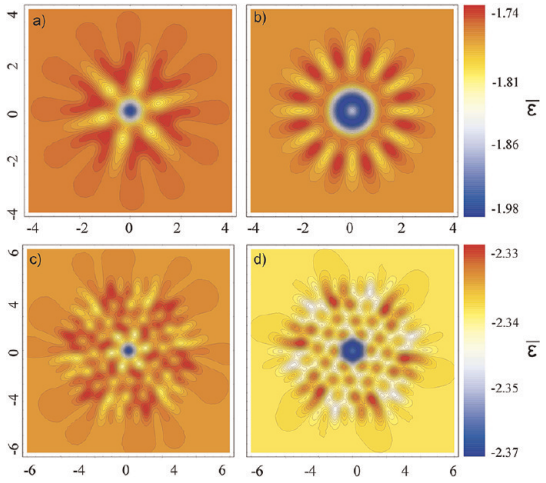

Figure 5. The total energy per particle (contour plot) of two systems of plaques shifted with respect to each other. In panels a and b, we show the energy of equal-size plaques, $M = 1$, with dipoles circulating in the opposite (left) and (right) the same directions. In panels c and d, the same is shown for plaques of different sizes, $M = 1$ and $M = 3$. The NP-diameter is chosen as the unit of shifts on the axes.

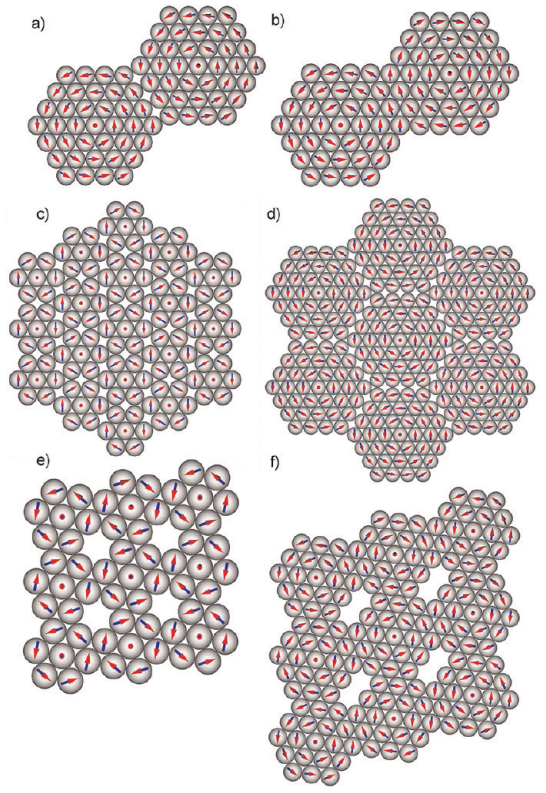

Figure 6. Two plaques connected by (a) the s-type junction and (b) the o-type junction. Lattices of connected plaques: (c) 19 plaques of $M = 1$ plaques assembled with the s-type junctions, (d) 7 plaques of $M = 3$ plaques assembled with the s-type junctions, (e) 9 plaques of $M = 1$ plaques assembled by the o-type junctions, (f) 9 plaques of $M = 2$ plaques assembled with the o-type junctions.

energy profiles for different sizes of plaques. As the plaques rotate, they acquire intermediate states between sh and hcp lattices, some of which are locally

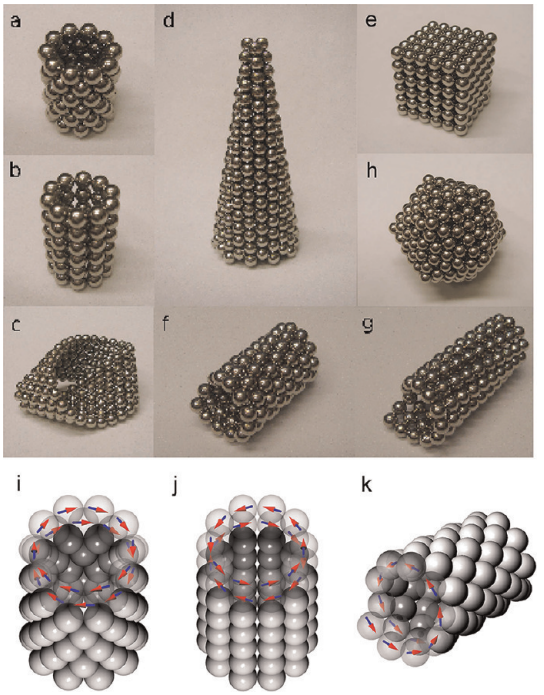

Figure 7. Magnetic particles arranged in a variety of structures: (a) tube with close-packing lattice, (b) tube with simple cubic packing lattice, (c) Möbius strip, (d) conical close-packing structure, (e) simple cubic lattice, (f) chiral tube with close-packing structure with parallel circulation of dipoles, (g) chiral tube simple cubic packing structure with antiparallel dipolar circulation, (h) hollow icosahedral structure, (i) close-packing tube, (j) simple cubic tube, and (k) chiral tube with close-packing structure with the circulation of dipoles shown.

stable. These configurations can be identified with the formation of the Moire pattern.[81]

Next, we explore the potential energy profile as a function of a mutual shift of the two plaques. In Figure 5 (top and bottom), we visualize these profiles for two different systems. The first one is formed by two identical plaques ($M = 1$, Figure 1 (top)) sitting on the top of each other, oriented in the same way, and mutually shifted in the common plane, while the distance between the plaques is constant. In the second system, the sizes of the two plaques are different ($M = 1$ and $M = 3$). The four insets show the potential energy when the plaques with the same (right) and opposite (left) circulations are shifted one with respect to the other (the coordinates are plotted in the units of the particle diameter).

When the vertical axis of both plaques coincide, the plaques are in the sh configuration, corresponding to the (0,0) center of coordinates in Figures 5a–d. This center is the most stable point for the opposite orientations of dipoles (left). For the same dipole orientation (right), the most stable configurations lie on the circle with the radius of $r = 1/\sqrt{3}$, where we can find hcp (fcc) arrangements, except of the slightly larger distance between the plaques. Once we leave the area close to the (0,0) center, a number of small local minima can be

TABLE 3. Binding Energies between Honeycomb Plaques Calculated per Particle at the Boundary[a]

	circ. 1(7)		circ. 2(19)		circ. 3(37)		circ. 4(61)	
	same	opp.	same	opp.	same	opp.	same	opp.
$\bar{\varepsilon}_{boundary}$	−0.24	−0.20	−0.20	−0.16	−0.21	−0.12	−0.22	−0.09

[a] Different sizes and mutual orientation of circulating dipoles are considered (same/opp. = dipolar circulation of neighboring plaques).

observed, depending on the system size. The magnetic vortices in both plaques break the translational symmetry of these systems at any plaque size.

Planar Lattices Built from Particle Plaques. We continue to study periodic systems assembled from the above plaques. In Figure 6a,b, we show two plaques in two stable configurations, with the same and opposite circulations of dipoles at the particle boundaries as in Figure 2, respectively. In Table 3, we give the binding energies between plaques per particle at the boundary for two plaques of different sizes and dipole orientations (for example, the $M = 3$ plaques have eight particles at their boundary); the same and opposite orientations of dipoles in neighboring plaques favor different boundaries. As the plaques become larger, the binding energy per particle at the boundary should saturate.

We also extend this plaque binding to lattices. In Figure 6c,d, we show the lattices formed of $M = 1$ and $M = 3$ hexagonal plaques having the same (s) and opposite (o) circulations. When the magnetic fluxes circulate in the same direction, the plaque is the elementary cell of the 2D crystal. In this case, the s-type junctions allow the formation of structures without vacancies. On the other hand, when the plaques are connected with the o-type junctions, as in Figure 6 e,f, their magnetic fluxes circulate in alternating directions, so the elementary cell is formed by four neighboring plaques, the same-type junctions. The o-type junctions lead to lattices with (periodic) vacancies. One can also imagine 2D lattices with combined s and o-types of junctions. Some of them can tend to form partially corrugated lattices.

Tubular Arrangements of Dipolar Particles. Particles with dipolar coupling can also form various tubular structures, which can be assembled into lattices. Typically, tubular structures can form rings, where the dipoles circulate around the circumference. Again, these rings can be connected with the s and o-type junctions, as shown in Figure 7a,b. The dipoles circulate in the directions shown in Figure 7i,j.

Other more exotic structures can also be formed. For example, we can assemble chiral tubular structures of dipolar particles, observed experimentally.[82] These helices can have different pitch, which can be equal integer numbers for the s-type junctions, as shown in Figure 7f,k, and even numbers for the o-type junctions, as shown in Figure 7g. The s-type tubular structures have nonzero fluxes oriented along their axes, proportional to the pitch, while the o-type structures have almost zero fluxes. One can even form knots based on a right-handed or a left-handed Möbius strip with the s and o-type junctions, as depicted in Figure 7c. The dipolar particles might also be stabilized to form conical structures, as illustrated in Figure 7d. The dipoles circulate in a uniform direction spirally around the cone, similar to that of the close-packed chiral nanotube.

Apart from planar and tubular structures, other stable structures can be assembled from dipolar particles. In Figure 7e, we show a simple cubic crystallite. Within each layer of the lattice, the dipoles in each chain are antiparallel to the neighboring chains, as well as to those in the layers above or below it. The stabilization takes part in similar way as in the structures discussed before. In Figure 7h, we also show a hollow icosahedral structure, which is formed by hexagons and pentagons, with closed magnetic fluxes. The direction of dipole circulation in each face is the same, which makes the structure chiral.

CONCLUSIONS

We have described a rich spectrum of clusters and lattices that can be stabilized from particles with electric and magnetic dipole−dipole coupling. The dipolar coupling between large particles should be strong enough to control both their dipolar and lattice structures. We show in a phase diagram the effect of interparticle vdW coupling and entropic effects associated with different lattice arrangements at finite temperatures. The obtained results can provide guidance for the self-assembly of unique structures at different scales, but their formation might require a careful control of the particle kinetics. The assembled particles can have applications as new materials for electronics, magnetism, and optics.

Conflict of Interest: The authors declare no competing financial interest.

REFERENCES AND NOTES

1. Murray, C. B.; Sun, S.; Doyle, H.; Betley, T. Monodisperse 3d Transition-Metal (Co, Ni, Fe) Nanoparticles and Their Assembly into Nanoparticle Superlattices. *Mater. Res. Soc. Bull.* **2001**, *26*, 985–991.
2. Alivisatos, A. P. Semiconductor Clusters, Nanocrystals, and Quantum Dots. *Science* **1996**, *271*, 933–937.
3. Manna, L.; Scher, E. C.; Alivisatos, A. P. Synthesis of Soluble and Processable Rod-, Arrow-, Teardrop-, and Tetrapod-Shaped CdSe Nanocrystals. *J. Am. Chem. Soc.* **2000**, *122*, 12700–12706.
4. Peng, X.; Manna, L.; Yang, W.; Wickham, J.; Scher, E.; Kadavanich, A.; Alivisatos, A. P. Shape Control of CdSe Nanocrystals. *Nature* **2000**, *404*, 59–61.
5. Puntes, V. F.; Zanchet, D.; Erdonmez, C. K.; Alivisatos, A. P. Synthesis of hcp-Co Nanodisks. *J. Am. Chem. Soc.* **2002**, *124*, 12874–12880.
6. Jun, Y.-w.; Casula, M. F.; Sim, J.-H.; Kim, S. Y.; Cheon, J.; Alivisatos, A. P. Surfactant-Assisted Elimination of a High Energy Facet as a Means of Controlling the Shapes of TiO_2 Nanocrystals. *J. Am. Chem. Soc.* **2003**, *125*, 15981–15985.

7. Li, X.; Sun, Z. Synthesis of Magnetic Polymer Microspheres and Application for Immobilization of Proteinase of Balillus Sublitis. *J. App. Polym. Sci.* **1995**, *58*, 1991–1997.
8. Min, Y.; Akbukut, M.; Kristiansen, K.; Golan, Y.; Israelachvili, J. The Role of Interparticle and External Forces in Nanoparticle Assembly. *Nat. Mater.* **2008**, *7*, 527–538.
9. Murray, C. B.; Kagan, C. R.; Bawendi, M. G. Self-Organization of CdSe Nanocrystallites into 3-Dimensional Quantum-Dot Superlattices. *Science* **1995**, *270*, 1335–1338.
10. Kovalenko, M. V.; Scheele, M.; Talapin, D. V. Colloidal Nanocrystals with Molecular Metal Chalcogenide Surface Ligands. *Science* **2009**, *324*, 1417–1420.
11. Murray, C. B.; Kagan, C. R.; Bawendi, M. G. Synthesis and Characterization of Monodisperse Nanocrystals and Close-Packed Nanocrystal Assemblies. *Annu. Rev. Mater. Sci.* **2000**, *30*, 545–610.
12. Puntes, V. F.; Krishnan, K. M.; Alivisatos, A. P. Colloidal Nanocrystal Shape and Size Control: The Case of Cobalt. *Science* **2001**, *291*, 2115–2117.
13. Burda, C.; Chen, X.; Narayanan, R.; El-Sayed, M. A. Chemistry and Properties of Nanocrystals of Different Shapes. *Chem. Rev.* **2005**, *105*, 1025–1102.
14. Ku, J.; Aruguete, D. M.; Alivisatos, A. P.; Geissler, P. L. Self-Assembly of Magnetic Nanoparticles in Evaporating Solution. *J. Am. Chem. Soc.* **2011**, *133*, 838–848.
15. Snezhko, A.; Aranson, I. S. Magnetic Manipulation of Self-Assembled Colloidal Asters. *Nat. Mater.* **2011**, *10*, 698–703.
16. Hao, Y.; Kondoh, H.; Shimojo, M.; Sako, E. O.; Ozaki, N.; Kogure, T; Ohta, T. High-Yield Preparation of Uniform Cobalt Hydroxide and Oxide Nanoplatelets and Their Characterization. *J. Phys. Chem. B* **2005**, *109*, 19094–19098.
17. Li, M.; Schnablegger, H.; Mann, S. Coupled Synthesis and Self-Assembly of Nanoparticles to Give Structures with Controlled Organization. *Nature* **1999**, *402*, 393–395.
18. Boal, A. K.; Ilhan, F.; DeRouchey, J. E.; Thurn-Albrecht, T.; Russell, T. P.; Rotello, V. Self-Assembly of Nanoparticles into Structured Spherical and Network Aggregates. *Nature* **2000**, *404*, 746–748.
19. Special issue: Nanostructured Materials. *Chem. Mater.* **1996**, *8*, (5).
20. Shi, J.; Gider, S.; Babcock, K.; Awschalom, D. D. Magnetic Clusters in Molecular Beams, Metals, and Semiconductors. *Science* **1996**, *271*, 937–941.
21. Petit, C.; Taleb, A.; Pileni, M. P. Self Assembled in 2D of Cobalt Nanosized Particles. *Adv. Mater.* **1998**, *10*, 259–261.
22. Yamamuro, S.; Farrell, D. F.; Majetich, S. A. Direct Imaging of Self-Assembled Magnetic Nanoparticles: Phase Stability and Magnetic Effects on Morphology. *Phys. Rev. B* **2002**, *65*, 224431.
23. Sun, S. Recent Advances in Chemical Synthesis, Self-Assembly, and Applications of FePt Nanoparticles. *Adv. Mater.* **2006**, *18*, 393–403.
24. Motte, L.; Billoudet, F.; Pileni, M. P. Self-Assembled Monolayer of Nanosized Particles Differing by Their Sizes. *J. Phys. Chem.* **1995**, *99*, 16425–16429.
25. Chen, C.-F.; Tzeng, S.-D.; Chen, H.-Y.; Lin, K.-J.; Gwo, S. Tunable Plasmonic Response from Alkanethiolate-Stabilized Gold Nanoparticle Superlattices: Evidence of Near-Field Coupling. *J. Am. Chem. Soc.* **2007**, *130*, 824–826.
26. Kodama, R. H. Magnetic Nanoparticles. *J. Magn. Magn. Mater.* **1999**, *200*, 359–372.
27. Asakura, S.; Oosawa, F. On Interaction between Two Bodies Immersed in a Solution of Macromolecules. *J. Chem. Phys.* **1954**, *22*, 1255–1256.
28. Asakura, S.; Oosawa, F. Interaction between Particles Suspended in Solutions of Macromolecules. *J. Polym. Sci.* **1958**, *XXXIII*, 183–192.
29. Bishop, K. J. M.; Wilmer, C. E.; Soh, S.; Grybowski, B. A. Nanoscale Forces and Their Uses in Self-Assembly. *Small* **2009**, *5*, 1600–1630.
30. Shevchenko, E. V.; Talapin, D. V.; Kotov, N. A.; O'Brien, S.; Murray, C. B. Structural Diversity in Binary Nanoparticle Superlattices. *Nature* **2006**, *439*, 55–59.
31. Titov, A. V.; Král, P. Modeling the Self-Assembly of Colloidal Nanorod Superlattices. *Nano Lett.* **2008**, *8*, 3605–3612.
32. Ohara, P. C.; Leff, D. V.; Heath, J. R.; Gelbart, W. M. Crystallization of Opals from Polydesperse Nanoparticles. *Phys. Rev. Lett.* **1995**, *75*, 3466–3469.
33. Chen, Z.; Moore, J.; Radtke, G.; Sirringhaus, H.; O'Brien, S. Binary Nanoparticle Superlattices in the Semiconductor–Semiconductor System: CdTe and CdSe. *J. Am. Chem. Soc.* **2007**, *129*, 15702–15709.
34. Korgel, B. A.; Fullam, S.; Connolly, S.; Fitzmaurice, D. Assembly and Self-Organization of Silver Nanocrystal Superlattices: Ordered Soft Spheres. *J. Phys. Chem. B* **1998**, *102*, 8379–8388.
35. Talapin, D. V.; Shevchenko, E. V.; Murray, C. B.; Titov, A. V.; Král, P. Dipole–Dipole Interactions in Nanoparticle Superlattices. *Nano Lett.* **2007**, *7*, 1213–1219.
36. He, J.; Lin, X. -M.; Chan, H.; Vukovic´, L.; Král, P.; Jaeger, H. M. Diffusion and Filtration Properties of Self-Assembled Gold Nanocrystal Membranes. *Nano Lett.* **2011**, *11*, 2430–2435.
37. Li, L.-S.; Alivisatos, A. P. Origin and Scaling of the Permanent Dipole Moment in CdSe Nanorods. *Phys. Rev. Lett.* **2003**, *90*, 097402.
38. Awschalom, D. D.; DiVincenzo, D. P. Complex Dynamics of Mesoscopic Magnets. *Phys. Today* **1995**, *48*, 43–48.
39. Haun, J. B.; Yoon, T. J.; Lee, H.; Weissleder, R. Magnetic Nanoparticle Biosensors. *WIREs Nanomed. Nanobiotechnol.* Wiley 2010, 2, 291–304.
40. Petukhov, V.; Zhikharev, V.; Ibragimova, M.; Zheglov, E.; Bazarov, V.; Khaibullin., V. I. Ion Synthesis of Thin Granular Ferromagnetic Films in Polymethylmethacrylate. *Solid State Commun.* **1996**, *97*, 361–364.
41. Polyak, B.; Fishbein, I.; Chorny, M.; Alferiev, I.; Williams, D.; Yellen, B. Magnetically Driven Plasmid DNA Delivery with Biodegradable Polymeric Nanoparticles. *The FASEB J.* **2007**, *21*, 2510–2519.
42. Miller, M. A.; Wales, D. J. Novel Structural Motifs in Clusters of Dipolar Spheres: Knots, Links, and Coils. *J. Phys. Chem. B* **2005**, *109*, 23109–23112.
43. Lin, X.-M.; Samia, A. C. S. Synthesis, Assembly and Physical Properties of Magnetic Nanopaticles. *J. Magn. Magn. Matter* **2006**, *305*, 100–109.
44. Terheiden, A.; Dmitrieva, O.; Acet, M.; Mayer, C. Magnetic Field Induced Self-Assembly of Gas Phase Prepared FePt Nanoparticles. *Chem. Phys. Lett.* **2006**, *431*, 113–117.
45. Lévy, J. C. Two-Dimensional Arrangements of Magnetic Nanoparticles. *Phys. Rev. B* **2003**, *67*, 064409.
46. Weis, J. J.; Levesque, D. Chain Formation in Low Density Dipolar Hard Spheres: A Monte Carlo Study. *Phys. Rev. Lett.* **1993**, *71*, 2729–2732.
47. Puntes, V. F.; Krishnan, K. M. Synthesis, Self-Assembly, and Magnetic Behavior of a Two-Dimensional Superlattice of Single-Crystal ε-Co Nanoparticles. *Appl. Phys. Lett.* **2001**, *78*, 2187–2189.
48. Golosovsky, M.; Saado, Y.; Davidov, D. Self-Assembly of Floating Magnetic Particles into Ordered Structures: A Promising Route for the Fabrication of Tunable Photonic Band Gap Materials. *Appl. Phys. Lett.* **1999**, *75*, 4168–4170.
49. Petit, C.; Taleb, A.; Pileni, M. P. Cobalt Nanosized Particles Organized in a 2D Superlattice: Synthesis, Characterization, and Magnetic Properties. *J. Phys. Chem. B* **1999**, *103*, 1805–1810.
50. Tripp, S. L.; Pusztay, S. V.; Ribbe, A. E.; Wei, A. Self-Assembly of Cobalt Nanoparticle Rings. *J. Am. Chem. Soc.* **2002**, *124*, 7914–7915.
51. Nayak, S. K.; Weber, S. E.; Jena, P. Relationship Between Magnetism, Topology, and Reactivity of Rh Clusters. *Phys. Rev. B* **1997**, *56*, 8849–8854.
52. Wildberger, K.; Stepanyuk, V. S.; Lang, P.; Zeller, R.; Dederichs, P. H. Magnetic Nanostructures: 4 *d* Clusters on Ag (001). *Phys. Rev. Lett.* **1995**, *75*, 509–512.
53. Vedmedenko, E. Y.; Ghazali, A.; Lévy, J. C. S. Magnetic Vortices in Ultrathin Films. *Phys. Rev. B* **1999**, *59*, 3329–3332.

54. Gubin, S. P.; Dzhardimalieva, G. I.; Eremenko, I. L.; Filinova, E.Yu.; Grebenshchikov, Yu.B.; Kiskin, M. A.; Khomutov, G. B.; Kliava, J.; Koksharov, Yu. A.; Kolesnichenko, V. L. *et al. Magnetic Nanoparticles*; Wiley-VCH Verlag GmbH&Co.: KGaA, Weinheim, 2009.
55. Graf, C.; Vossen, D. L. J.; Imhof, A.; van Blaaderen, A. A General Method To Coat Colloidal Particles with Silica. *Langmuir* **2003**, *19*, 6693–6700.
56. Chen, L. X.; Liu, T.; Thurnauer, M. C.; Csencsits, R.; Rajh, T. Fe_2O_3 Nanoparticle Structures Investigated by X-ray Absorption Near Edge Structure, Surface Modifications, and Model Calculations. *J. Phys. Chem. B* **2002**, *106*, 8539–8546.
57. Lee, S.-Y.; Harris, M. T. Surface Modification of Magnetic Nanoparticles Capped by Oleic Acids: Characterization and Colloidal Stability in Polar Solvents. *J. Colloid Interface Sci.* **2006**, *293*, 401–408.
58. Gu, S.; Shiratori, T.; Konno, M. Synthesis of Monodisperse, Magnetic Latex Particles with Polystyrene Core. *Colloid Polym. Sci.* **2003**, *281*, 1076–1081.
59. Skomski, R. Nanomagnetics. *J. Phys.: Condens. Matter* **2003**, *15*, R841–R896R.
60. Beleggia, M.; Tandon, S.; Zhu., Y.; De Graef, M. On the Magnetostatic Interactions between Nanoparticles of Arbitrary Shape. *J. Magn. Magn. Mater.* **2004**, *278*, 270–284.
61. Zhang, Z.; Glotzer, S. Self-Assembly of Patchy Particles. *Nano Lett.* **2004**, *4*, 1407–1413.
62. Xia, Y.; Nguyen, T. D.; Yang, M.; Lee, B.; Santos, A.; Podsiadlo, P.; Tang, Z.; Glotzer, S. C.; Kotov, N. A. Self-Assembly of Self-Limiting Monodisperse Supraparticles from Polydisperse Nanoparticles. *Nat. Nanotechnol.* **2011**, *6*, 580–587.
63. Glotzer, S. C.; Solomon, M. J. Anisotropy of Building Blocks and Their Assembly into Complex Structures. *Nat. Mater.* **2007**, *6*, 557–562.
64. Jonsson, T.; Nordblad, P.; Svedlindh, P. Dynamic Study of Dipole−Dipole Interaction Effects in a Nanoparticle System. *Phys. Rev. B* **1998**, *57*, 497–504.
65. Vargas, J. M.; Nunes, W. C.; Socolovsky, L. M.; Knobel, M.; Zanchet, D. Effect of Dipolar Interaction Observed in Iron-Based Nanoparticles. *Phys. Rev. B* **2005**, *72*, 184428.
66. Plumer, M. L.; Rogers, M. C.; Meloche, E. Micromagnetic Simulations of Interacting Dipoles on an fcc Lattice: Application to Nanoparticle Assemblies. *J. Phys.: Condens. Matter* **2010**, *22*, 296007.
67. Grzelczak, M.; Vermant, J.; Furst, E. M.; Liz-Marzán, L. M. Direct Self-Assembly of Nanoparticles. *ACS Nano* **2010**, *7*, 3591–3605.
68. Šafařík, I.; Šafaříková, M. Magnetic Nanoparticles and Biosciences. *Monats. Chem.* **2002**, *133*, 737–759.
69. Leunissen, M. E.; Christova, Ch.G.; Hynnenen, A.-P.; Royall, C. P.; Campbell, A. I.; Imhov, A.; Dijkstra, M.; van Roij, R.; van Blaaderen, A. Ionic Colloidal Crystals of Oppositely Charged Particles. *Nature* **2005**, *437*, 235–240.
70. Hamaker, H. C. The London van der Waals Attraction between Spherical Particles. *Physica* **1937**, *4*, 1058–1072.
71. Zhu, J.-G.; Zheng, Y. F.; Prinz, G. A. Ultrahigh Density Vertical Magnetoresistive Random Access Memory. *J. Appl. Phys.* **2000**, *87*, 6668–6673.
72. Aizpurua., J.; Hanarp, P.; Sutherland, D. S.; Käll, M.; Bryant, G. W.; Garcia de Abajo, F. J. Optical Properties of Gold Nanorings. *Phys. Rev. Lett.* **2003**, *90*, 057401.
73. Jackson, L. D. *Classical Eletrodynamics* **1975**, 143.
74. Claesson, E. M.; Erné, B. H.; Bakelaar, I. A.; Kuipers, B. W. M.; Philipse, A. P. Measurement of the Zero-Field Magnetic Dipole Moment of Magnetizable Coloidal Silica Spheres. *J. Phys.: Condens. Matter* **2007**, *19*, 41–54.
75. Bergrstrom, L. Hamaker Constants of Inorganic Materials. *Adv. Coll. and Interf. Sci* **1997**, *70*, 125–169.
76. Woodcock, L. V. Entropy Difference Between the Face-Centred Cubic and Hexagonal Closed-Packed Crystal Structures. *Nature* **1997**, *385*, 141–143.
77. Hoover, W. H.; Ree, F. H. Melting Transition and Communal Entropy for Hard Spheres. *J. Chem. Phys.* **1968**, *49*, 3609–3617.
78. Esbjørn, P. O.; Jensen, E. J.; Kristensen, W. D.; Martin, J. W.; Pedersen, L. B. Entropy of fcc and hcp Lattices: Comparison of H Theorem Method with Vibrational Analysis. *J. Comput. Phys.* **1973**, *12*, 289–307.
79. Speedy, R. J. Pressure and Entropy of Hard-Sphere Crystals. *J. Phys.: Condens. Matter* **1998**, *10*, 4387–4391.
80. Whitelam, S.; Feng, E. H.; Hagan, M.; Geissler, P. The Role of Collective Motion in Examples of Coarsening and Self-Assembly. *Soft Matter* **2009**, *5*, 1251–1262.
81. Majiles Ara, M. H.; Golzarian, R.; Javadi, Z.; Sahraei, R. Nonlinear Optical Characterization of CdTe Nano Particles Using Moir Deflectometry Method. *Phys. Proc.* **2011**, *19*, 482–486.
82. Harada, T.; Simeon, F.; Vander Sande, J. B.; Hatton, T. A. Formation of Magnetic Nanotubes by the Cooperative Self-Assembly of Chiral Amphiphilic Molecules and Fe_3O_4 Nanoparticles. *Phys. Chem. Chem. Phys.* **2010**, *12*, 11938.